Realistic Strategy for Design Optimization of Halide Perovskite Solar Cell via tailoring bands offset engineering and Back Contact

H. Bencherif [1,*], F. Meddour[1], M. H. Elshorbagy[2,3], T. Bendib[1], A. Cuadrado[3], M. A. Abdi[1], S. Kouda[1], J. Alda[3]

[1] HNS-RE2SD, Higher National School of Renewable Energy, Environment & Sustainable development, Batna, Algeria,
[2] Physics Department, Faculty of Science, Minia University, El Minya, 61519, Egypt.
[3] Applied Optics Complutense Group, Faculty of Optics and Optometry, University Complutense of Madrid, 28037, Madrid, Spain.

* E-mail: hichem.bencherif@univ-batna2.dz, hichem.bencherifeln@gmail.com

Abstract

Perovskite is one of the most a potential material for photovoltaic devices. Its development relies mostly on the material engineering to enhance both performance and stability. In this work, an optimal design of an n-i-p $FAPbI_3$ perovskite solar cell (PSC) is investigated. Various alternative charge transport layers (CTLs) are evaluated, where the findings show that Copper oxide Cu_2O as hole transport material and Magnesium Zinc Oxide MgZnO alloy as electron transport material are the best candidates. Besides, the device performance is optimized using a mixed cation and anion based on $(FAPbI_3)_{1-x}(MAPbBr_3)_x$ as an absorber layer. Finally, suitable band offset alignment was established via tuning the affinities of both CTLs and the addition of an appropriate back electrode material. The optimized FTO/MgZnO/$FAPbI_{3(0.85)}$ $MAPbBr_{3(0.15)}$/Cu_2O/Ni PSC reaches a conversion efficiency as high as 25.86%. According to the recommended optimization technique, there is plenty of space for enhancement.

Key words: ($FAPbI_3)_{1-x}(MAPbBr_3)_x$ perovskite solar, Charge transport layers, Band alignment, back electrode, performance optimization.

Introduction

During the last ten years, hybrid organic-inorganic metal halide perovskite solar cells (PSCs) have revealed remarkable performance gains. With power conversion efficiency (PCE) record higher than 25 % [1], PSCs are already intriguingly competing with other known photovoltaic material systems at a significantly lower manufacturing cost [2]. The outstanding photovoltaic efficiency of PSCs is attributed to the hybrid perovskite material, which has high drift mobility, a low binding energy of exciton, effective charge collection, long charge carrier diffusion lengths, distinguished absorption coefficient, and [3]. Another feature of perovskite materials that can support the potential of PSC performance to achieve its theoretical maximum is the decreased bulk recombination rates, particularly the non-radiative component [4]. Considering these outstanding properties, the second step in boosting PSC performance will need research and refinement of other PSC constituents, particularly the charge transport layers (CTLs), to reduce interfacial recombination, a substantial degradation cause [5]. CTL study has thus concentrated on conductivity / mobility [6], photocurrent hysteresis [7], interfacial defect passivation [8], film morphology, [9] electronic structure, and device stability [5]. Since long ago, the CTL electronic configuration, in particular, has been the focus of research. This layer influences the performance of the device, and a previous study has found fewer damaging consequences due to possible interfacial dipoles from ionic accumulation close to the interface [10]. This lack of information regarding the importance of CTL electronic structure creates a problem when it comes to enhancing the device's capabilities. Nevertheless, resolving this issue by an effective experimental assessment would be time consuming and expensive. Therefore, the utilization of device simulations allow the comprehensive examination of the influence of each component of PSCs as well as alternative combinations.

Minemoto and Murata conducted a simulation research that gives insight on this subject, however, a global optimization is needed [11]. Furthermore, beyond the fundamental current density-voltage (*J-V*) measurements, information from the fundamental physical mechanisms is extremely useful in understanding and guiding studies.

In this work, we demonstrate that CTLs with appealing optical properties, good conductivity, and suitable band structure alignment significantly improve the device performance with the presence of defects at CTL/perovskite interfaces. It also enhances the device light absorption, and consequently maintains high PCE. High-performance PSCs have been demonstrated using hole transport layers (HTLs) with deep energy levels, such as Cu_2O, and shallow energy level electron transport layers (ETLs), such as ZnO, which have strong conductivity and high optical transparence [12]. With the endeavor of enhancing the PSC performance in terms of open circuit voltage, V_{OC}, a mixed PSC is investigated. Findings show that the usage of $(FAPbI3)_{0.85}$ $(MAPbBr_3)_{0.15}$ with optimum band gap (1.56 eV) and thickness (800 nm) increases the efficiency until reaching a value of 23.56 %. Besides, efficient CTL/PVK interfaces are critical for pushing PSC efficiency. The conduction band offset (CBO) and valence band offset (VBO) can be adjusted to achieve this performance. Researchers have demonstrated that the nature of ETL/PVK interface (spike or cliff structures) generated via changing the electron affinity of ETL can affect the performance of PSCs, and these band offsets are important for transport mechanism in PSCs [11]. To overcome the aforementioned problem, the magnesium doped zinc oxide ($Zn_{1-x}Mg_xO$) as ETL with adjusted affinity is a promising candidate for boosting the performance of the device via mitigating the effect of the interfacial defects. In the same way Cu_2O affinity can be tuned to optimize the band offset alignment in HTL/PVK interface. Moreover, a suitable metal contact with work function is investigated. These characteristics contribute to the improved performance of the PSCs we studied. Using enhanced EA_{ETL} (3.86 eV) and EA_{HTL} (3.7 eV) Ni as contact with work

function equal to 5.04 eV we can yield a PCE of 25.86 % for FTO/$Zn_{0.8}Mg_{0.2O}$/$(FAPbI_3)_{0.85}$ $(MAPbBr_3)_{0.15}$/Cu_2O/Ni structure with a short circuit current (J_{SC}) of 25.01 mA/cm^2, an open circuit voltage (*V*oc) of 1.23 V and a fill factor (*FF)* around 83.9 %. The proposed study offers a practical guideline for a realistic strategy to the CTL design and optimization of PSCs.

1- Device structure

Figure 1 depicts the n-i-p configuration of the studied perovskite formamidinium lead triiodide ($FAPbI_3$) based solar cell. It comprises, comprehensively, gold as a back contact, Spiro-OMeTAD as HTL material, an intrinsic $FAPbI_3$ perovskite material that serves as light harvesting material, and SnO_2 as ETL material. When the solar cell is illuminated, the perovskite layer is the region of exitons formation. The diffusion length of electrons (holes) and ETL (HTL) electrical characteristics are key factors for the dissociation and collection mechanisms. Exciton separation happens at CTLs/ perovskite interfaces. Electrons move to the ETL (n) area, whereas holes migrate to the HTL region (p). The electric field at ETL/perovskite and Perovskite/HTL interfaces is responsible for the dissociation and migration processes. **Table 1** recapitulates the input data for the reference PSC FTO/SnO_2/$FAPbI_3$/Spiro-OMeTAD/Au. An AM1.5G solar spectrum is considered for our simulation. The perovskite input parameters are obtained from the literature [13].

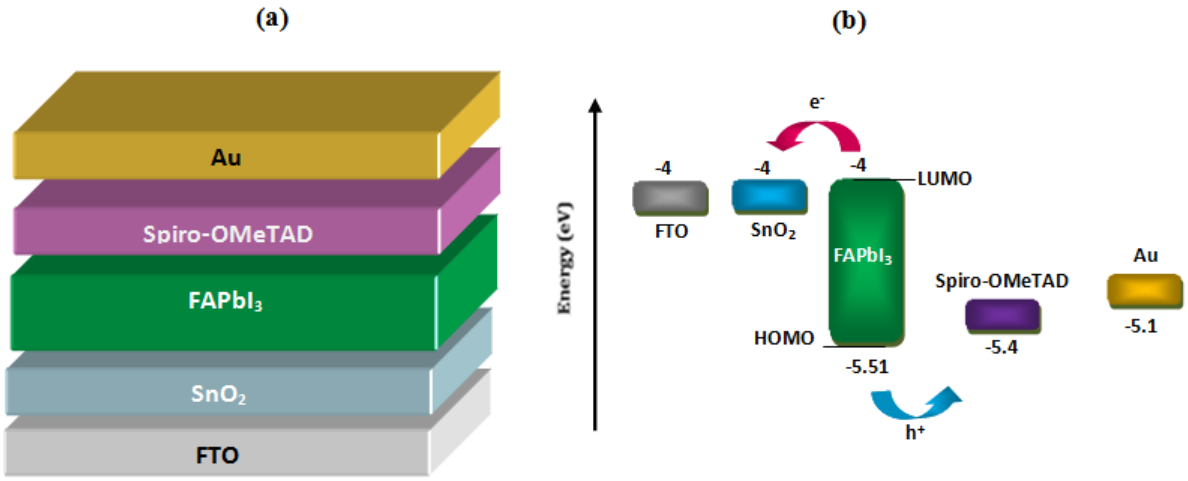

Figure 1. a) 3D cross-sectional view of the investigated FTO/SnO_2/$FAPbI_3$/Spiro-OMeTAD perovskite solar cell, b) Bands alignment between perovskite and CTLs.

2- Physical models and parameters

As a simulation software, SCAPS 1d was utilized [14]. The main semiconductor equations used in SCAPS are Poisson's (1) and the continuity equations for electrons (2) and holes (3), as shown below:

$$\frac{d}{dx}\left(\varepsilon(x)\frac{d\psi}{dx}\right)=q\left[p(x)-n(x)+N_D^+-N_A^-+p_t(x)-n_t(x)\right] \quad (1)$$

$$-\frac{1}{j}\frac{dJ_n}{dx}+R_n(x)-G(x)=0 \quad (2)$$

$$\frac{1}{j}\frac{dJ_p}{dx}+R_p(x)-G(x)=0 \quad (3)$$

were, ε and q denote the permittivity of the medium, and the electron charge, respectively. ψ represents the electrostatic potential and n (p) refers to the electrons (holes) concentration, n_t (p_t) represents the trapped electron (hole). N_D^+ (N_A^-) denotes the ionized donor-like (acceptor-like) doping concentration, R_n(x) (R_p(x)) represents the electrons (holes) recombination rate, the generation rate is symbolized by G(x), J_n (J_p) are the electron and hole current densities, respectively. In this simulation, a planar structure was employed, where the electron transport layer ETL was modeled by inspecting different materials such as SnO_2, ZnO, TiO_2, WO_3,

ZnSe. $FAPbI_3$ used as light harvester, and Spiro-OMeTAD as the hole transport material (HTM). The second step of this simulation we compare the effect of different HTM such as P_3HT, $CuSbS_2$, Cu_2O, NiO and Spiro-OMeTAD on the device performance. Moreover, gold (Au), aluminum (Al), silver (Ag), Tungsten (W), Molibiden (Mo)**,** Nickel (Ni)**,** Copper (Cu) were investigated as a back contact while keeping FTO as the front contact. **Table 1** summarizes the parameters values used in our simulation derived from literatures [13, 15-21]. The properties of both CTL/perovskite interfaces including interface defects are also incorporated in the modeling framework.

Table 1. FTO/SnO_2/$FAPbI_3$/Spiro-OMeTAD parameters with active cell area of 0.09 cm^2.

Parameters	**Symbol (unit)**	FTO	SnO_2	$FAPbI_3$	$MAPbBr_3$	spiro-MeOTAD
Electron affinity	χ (eV)	4	4	4 [16,17]	3.6 [17]	2.5
Band gap	E_g (eV)	3.5	3.5	1.48	2.3	2.9
Thickness	(nm)	500	70	350	/	200
Permittivity	ε_r	9	9	6.6 [18]	28.7 [20]	3
Effective density of states at Conduction Band (CB)	N_C (cm^{-3})	2.2×10^{18}	2.2×10^{17}	1.2×10^{19}	2.2×10^{18}	2.2×10^{18}
Effective density of states at Valence Band (VB)	N_V (cm^{-3})	2.2×10^{18}	2.2×10^{17}	2.9×10^{18}	1.9×10^{19}	2.2×10^{18}
Electron thermal velocity	*($cm\ s^{-1}$)*	1×10^{7}	1×10^{7}	1×10^{7}	1×10^{7}	1×10^{7}
Hole thermal velocity	*($cm\ s^{-1}$)*	1×10^{7}	1×10^{7}	1×10^{7}	1×10^{7}	1×10^{7}
μ_n	μ_n	20	20	2.7 [21]	24 [21]	1×10^{-4}
μ_p	μ_p	10	10	1.8 [19]	0.25-0.59 [21]	1×10^{-4}
N_A	N_A	/	/	1.3×10^{16}	1.3×10^{16}	1.3×10^{18}
N_D	N_D	1×10^{15}	1×10^{15}	1.3×10^{16}	1.3×10^{16}	/
Nt	*Nt* (cm^{-3})	1×10^{18}	1×10^{18}	4×10^{13}	4×10^{13} cm^{-3}	1×10^{15}

Table 2 recapitulates the parameters values used in our simulation for both ETL/$FAPbI_3$ and $FAPbI_3$/ HTL interfaces.

Table 2. interfaces properties.

Interface	Defect type	Energetic distribution	Defect energy level	Capture cross section electrons (holes)	Density
ETL/ FAPbI3	neutral	Single	Above VB	1×10^{-17} (1×10^{-18})	1×10^{11}

			max		
FAPbI3/HTL	neutral	Single	Above VB max	1×10^{-18} (1×10^{-19})	1×10^{11}

To account for the empirical absorption coefficient of the simulator, we must enter it from external files based on experimental results. **Figure 2** depicts the absorption coefficients of FTO, ETMs, and HTMs, which are connected to the extinction coefficient computed utilizing $\alpha=4\pi k/\lambda$ [22], while the absorption coefficient of the active layer was taken from experimental data [23]. **Figure 2** depicts the solar irradiance to evaluate the absorption coefficient of the investigated materials. The absorption coefficient specifies how deep light of a specific wavelength may pass into a substance before being absorbed. Engineers may utilize the absorption coefficient range of materials to help them choose which material to employ in their solar cell designs. It can be seen from figure that $FAPBI_3$ shows higher absorption coefficient in the visible range than MAPbI3, however, this later in contrast to FAPbI3 demonstrates an extended absorption to 800 nm. Besides, the ETL absorption coefficients are also shown in this figure. It is noticeable that attractive ETL material must be transparent permitting to high amount of photons to be absorbed. This fact will improve the photogeneration mechanism at the absorber and enhance the device efficiency.

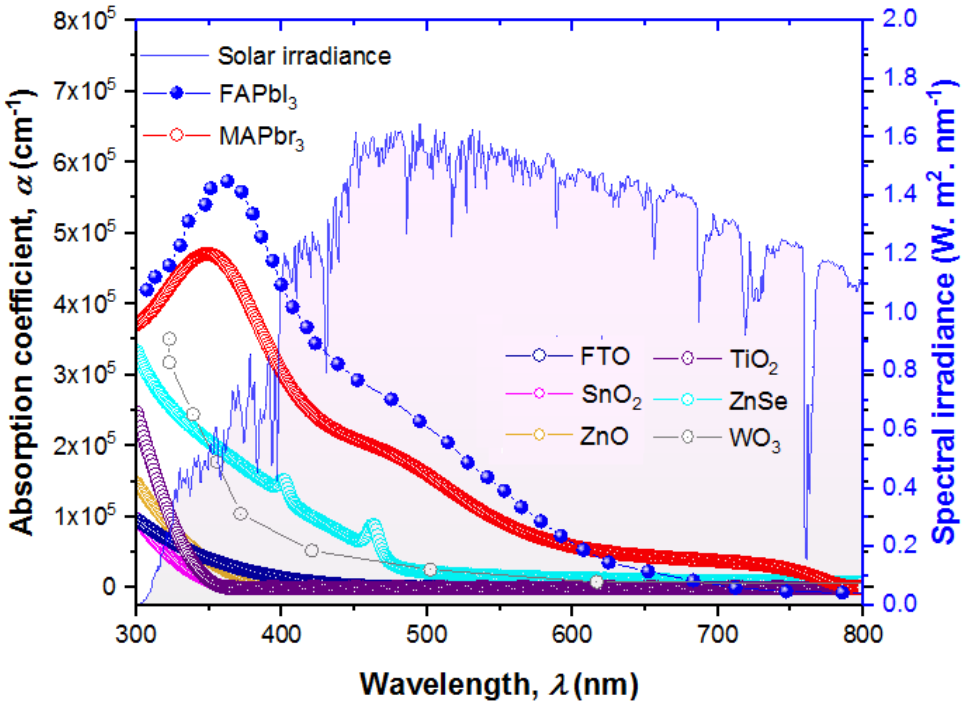

Figure 2. Absorption coefficients of different ETM materials and perovskites and solar spectral radiance as function of wavelength.

Similar to [24,25] the transfer matrix method (TMM) approach is employed to determine the generation rate of the structure and inserted into the software.

4. Results and discussion

Figure 3 depicts the examined PSC's simulated J-V characteristics acquired using data from tables 1 and 2. Assuming layer thicknesses and optical parameters are close to measurements, the optical-electrical modeling based on transfer matrix approach and drift diffusion concept could be capable to efficiently estimate the device behavior [16-21].

The *J-V* parameters of the reference FTO/SnO_2/$FAPbI_3$/Spiro-OMeTAD/Au perovskite solar cell are evaluated against experimental results to assess the correctness of the simulation model [13]. Figure 3 illustrates a remarkable coincidence, showing that the proposed framework is appropriate. The slight discrepancy was mostly attributable to the series resistance and the charges accumulated at the ETL/PVK and HTL/PVK interfaces. **Table 3** summarizes the results of both the simulated and experimental structures, including also the

fill factor (FF) and quantym efficiency of the structure. **Figure 3-b** depicts the studied structure's band diagram.

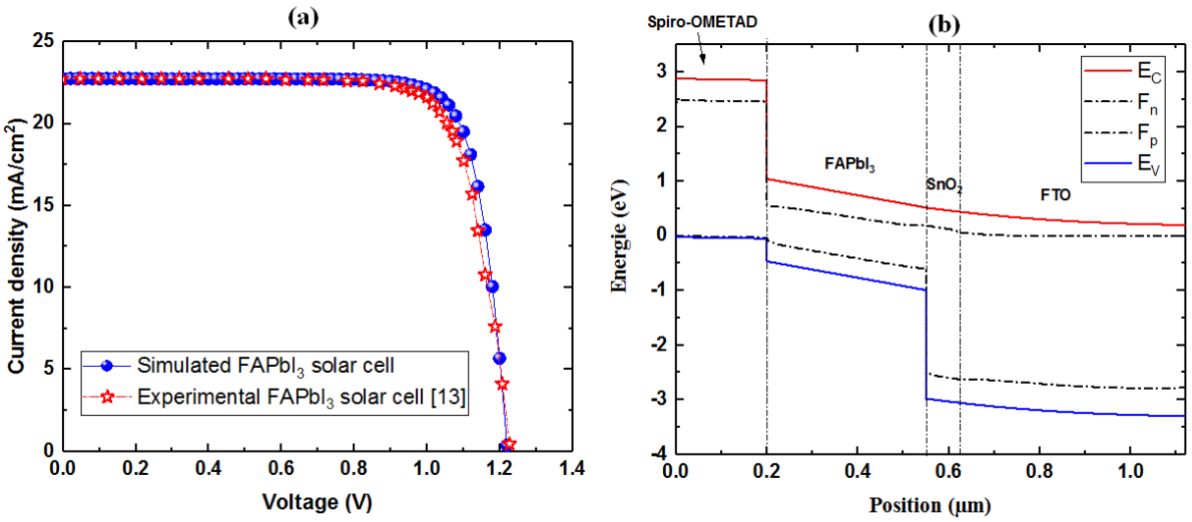

Figure 3. a) *I-V* characteristics, b) Band diagram of the investigated solar cell.

The band offset between SnO_2 and $FAPbI_3$ is matched in this figure, which may impact the separation process and therefore restrict the PCE. Whereas, SnO_2 guarantees an efficient hole blocking mechanism. Even if Spiro-OMeTAD is still the main component in highest efficient reported perovskites, its high hygroscopicity, tendency to crystallize, and vulnerability to both moisture and heat, justify the investigation of suitable and robust HTMs candidates as a vital task.

Table 3 Electrical outputs comparison of simulated and experimental perovskite solar cell.

	V_{OC} (V)	J_{SC} (mA/cm^{-2})	FF (%)	QE (%)
Experimental work [13]	1.2	22.6	77	21.4
Numerical simulation	1.21	22.96	79.17	22.17

4.1. PSC performance with Spiro-OMeTAD as HTM and several ETM candidates

ETM's task is to guarantee electron diffusion from the absorber $FAPbI_3$ into the front contact FTO through the built-in potential, and hence to the external circuit. This layer is essential for the diffusion-dissociation of the photogenerated charge carriers. TiO_2 is commonly utilized in devices, being the TiO_2 compact/TiO_2 mesoporous the most recent choice [26], however it requires a high temperature processing, which limits the application of

the device to flexible substrates and to the roll-to-roll production processes. To solve these issues, two types of ETMs were examined: the first with a elevated temperature of processing, like TiO_2, and the second with a low processing temperature, such as ZnO, ZnSe, WO_3, and SnO_2 [27-28]. Table 4 contains the input parameters of the simulated ETMs [24-29].

Table 4 Input parameters of ETMs.

Parameters	**Symbol (unit)**	ZnO	TiO_2	WO_3	ZnSe
Electron affinity	χ (eV)	4.16	4.26	3.8	4.39
Band gap	E_g (eV)	3.26	3.05	2.6	2.81
Thickness	(nm)	70	70	70	70
Relative permittivity,	ε_r	9	9	4.8	8.6
N_C	N_C	2.2×10^{18}	2.2×10^{18}	2.2×10^{21}	2.2×10^{18}
N_V	N_V	1.9×10^{19}	1.9×10^{19}	2.2×10^{21}	1.9×10^{19}
μ_n	μ_n	100	20	30	400
μ_p	μ_p	25	10	30	110
N_D	N_D	1×10^{18}	1×10^{18}	1×10^{18}	1×10^{18}
Nt	Nt	1×10^{15}	1×10^{15}	1×10^{15}	1×10^{15}

The J-V characteristics and the band diagrams alignment obtained from our simulation are presented in figure 4-a and 4-b. According to the figure, for the similar thickness of the ETMs, the performance of PSCs that utilize ZnO and SnO_2 was better compared to other candidates. Table 4 summarizes the figures of merit of the studied solar cell with different ETMs.

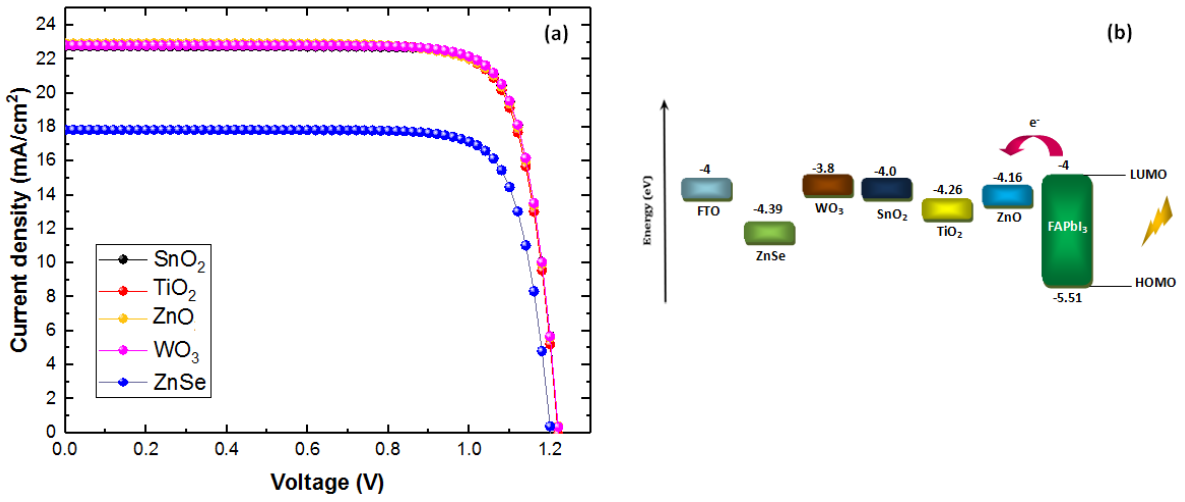

Figure 4. a) *J-V* characteristics comparison of different ETM candidates, b) alignment of the energy band diagrams for perovskite and other ETM candidates.

Table 5 Perovskite solar cell samples' figures of merit.

Perovskite samples	V_{OC} **(V)**	J_{SC} **(mA/cm^{-2})**	***FF* (%)**	***QE* (%)**
FTO/SnO_2/$FAPbI_3$/Spiro-OMeTAD	1.21	22.96	79.17	22.17
FTO/TiO_2/$FAPbI_3$/Spiro-OMeTAD	1.212	22.93	79.83	22.18
FTO/ZnO/$FAPbI_3$/Spiro-OMeTAD	1.22	22.93	79.92	22.36
FTO/WO_3/$FAPbI_3$/Spiro-OMeTAD	1.216	22.78	79.72	22.08
FTO/ZnSe/$FAPbI_3$/Spiro-OMeTAD	1.195	17.85	80.67	17.20

It can be deducted from **Figure 4-a**, that ZnO, or SnO_2, as ETM allows a higher current density than other ETMs. This is owing to the high transparence between 300 and 550 nm of both materials (see Fig. 2) as compared to other candidates which permits improved perovskite absorption. From figure 4, it is clearly shown that WO_3 and ZnO have the highest V_{OC}. This is owing to the appropriate energy band alignment and the higher electric field created at the interface with absorber layer which assures a reduced interfacial recombination rate and an efficient separation mechanism when compared to SnO_2. *FF* and *PCE* remains unchanged when the ETM thickness and doping increase. It can be noted that ETM thickness and doping have only a minor influence on the performance of the device. This fact is mainly owing to the high light penetration depth into the device which is higher than ETM thickness. Besides, the proposed model didn't take into account the parasitic losses dues to the ETL doping level, so, the obtained results can decrease with increased doping concentration.

4.1.1. The nature of different ETMs band engineering

The band diagram of the studied solar cell employing several ETM candidates is shown in **Figure 5**.

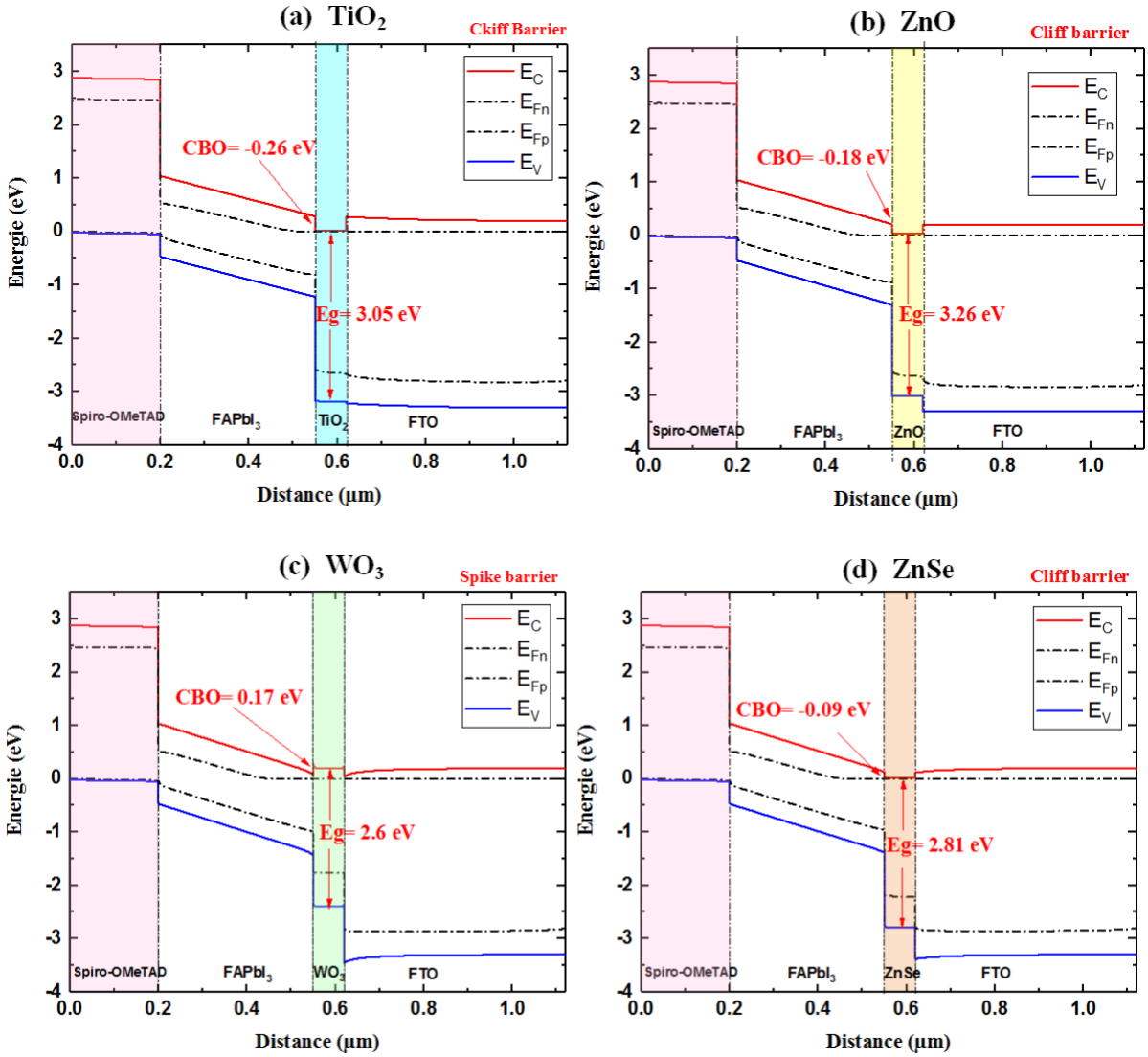

Figure 5 Band diagrams of the investigated solar for different ETM candidates, (a) TiO_2, (b) ZnO, (c) WO_3, (d) ZnSe.

Findings from figure 5 imply that ZnO and SnO_2 low processing temperature ETMs might be a viable choice for in PSCs device manufacturing efficiency. However, ZnO ETM can overcome problems such as the low electric field generated by SnO_2/PVK and the poor transparence of WO_3 in the mid UV band, allowing the device to function better. Furthermore, Mg or In Ga doped ZnO may be used to adjust the ZnO affinity and improve the band alignment offset [30].

4.2. PSC performance with ZnO as ETM and several HTM candidates

Due to its large hygroscopicity, inclination to crystalize, and sensitivity to both moisture and heat, the most widely employed hole transport layer, Spiro-OMeTAD, must be replaced. Up to this point, robust metal oxide carbon and other inorganic materials have been demonstrated as effective strategies for increasing device stability, although the PCE in these devices is still being tuned [31].

Figure 6-a depicts the *J-V* curves for ZnO (70 nm)/$FAPbI_3$PSCs (350 nm) based solar cell using different HTM (200 nm) candidates namely P_3HT, Cu_2O, $CuSbS_2$, NiO, and Spiro-OMeTAD. **Figure 6-b** shows PSC energy level diagrams with ZnO as the ETM and various inorganic and organic HTM that alter the VBO. The alignment of the energy levels in the solar cells is critical to their performance. For Perovskite solar cell scenario, photogenerated electrons are introduced into the ZnO conduction band, at the same time as holes migrate to the HTM. The photogenerated carriers are then collected at their corresponding contacts. For electrons extraction at the ETL/FAPbI3 interface, the electron affinity (EA) of ETL ought to be superior to that of perovskite, whereas the HTM's energy of ionization ought to be inferior to that of perovskite for efficient holes extraction at the HTM/FAPbI3 interface. The V_{OC} and J_{SC} are influenced by the energy level difference at the ETM/perovskite and perovskite/HTM interfaces. The input data for the simulated HTMs are listed in Table 4 [13, 32].

Table 6 Input parameters of HTMs.

Parameters	**Symbol (unit)**	P3HT	NiO	Cu_2O	$CuSbS_2$
Electron affinity	χ (eV)	3.1	1.8	3.2	4.2
Band gap	E_g (eV)	1.85	3.6	2.1	1.53
Thickness	(nm)	200	200	200	200
Relative permittivity,	ε_r	3.4	11	7.11	14.6
N_C	N_C	1×10^{22}	1.6×10^{19}	2.2×10^{18}	2×10^{18}
N_V	N_V	1×10^{22}	1.1×10^{19}	1.9×10^{19}	1×10^{19}
μ_n	μ_n	1×10^{-4}	50	3.4	49
μ_p	μ_p	1×10^{-3}	50	3.4	49
N_A	N_A	1×10^{18}	1×10^{18}	1×10^{18}	1×10^{18}
Nt	***Nt***	1×10^{14}	1×10^{14}	1×10^{15}	1×10^{15}

From **figure 6-a**, the best performing device uses Cu_2O as HTM, with a V_{OC} of 1.22 V, J_{SC} of 23.5 mA/cm^2, and *FF* of 83 percent, and an overall *PCE* of 23.8 percent. NiO was next, with a PCE of 23.67%, J_{SC} of 23.3 mA/cm2, V_{OC} of 1.224 V, and *FF* of 83 percent. $CuSbS_2$ also show a quite good behavior, with a *PCE* of 23.6 percent, a V_{OC} of 1.11 V, a J_{SC} of 24.38 mA/cm^2, and an *FF* of 87.2 percent.

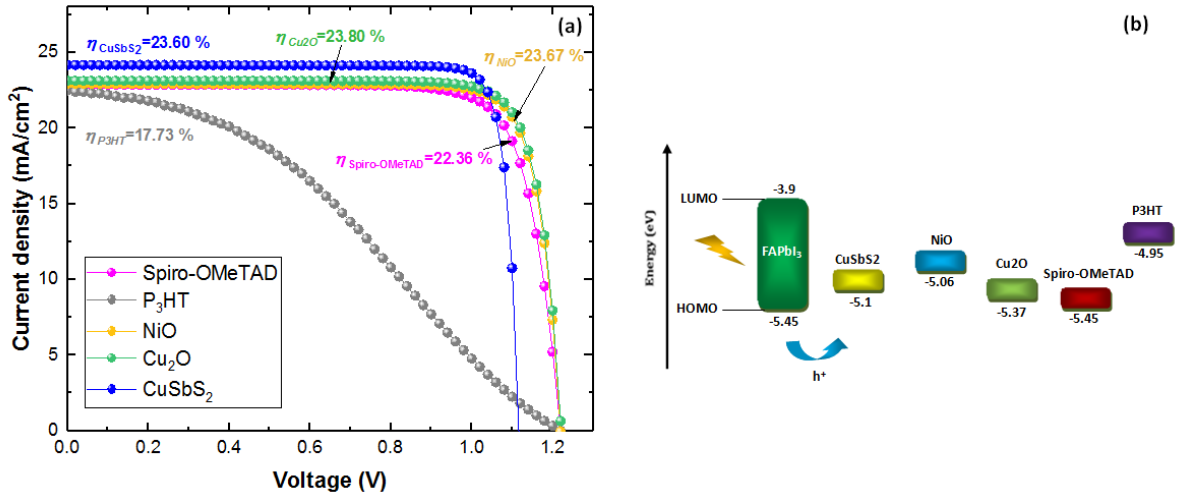

Figure 6. a) *I-V* characteristics comparison of different HTM candidates, b) alignment of the energy band diagrams for perovskite and other HTM candidates

When P_3HT was employed as the HTM, the PV performance was found to be rather poor, with a *PCE* of 17.73 percent, V_{OC} of 1.22 V, J_{SC} of 23 mA/cm2, and *FF* of 63.2 percent. **Table 5** recapitulate the electrical outputs of solar cell samples using different HTMs. Between all HTMs studied here, the highest PV performance was seen with Cu_2O as HTMs in PSCs utilizing ZnO as ETM. As compared to other HTMs/$FAPbI_3$ combinations, Cu2O/$FAPbI_3$ has an appropriate VBO. This permitted to enhance the V_{OC}.

Table 7 Perovskite solar cell samples' figures of merit.

Perovskite samples	J_{SC} (mA/cm^{-2})	V_{OC} (V)	FF (%)	QE (%)
FTO/ ZnO/$FAPbI_3$/Spiro-OMeTAD	22.93	1.22	79.92	22.36
FTO/ ZnO/$FAPbI_3$/P3HT	23	1.22	63.2	17.73
FTO/ZnO/$FAPbI_3$/NiO	23.3	1.224	83	23.67
FTO/ ZnO/$FAPbI_3$/Cu2O	23.5	1.22	83	23.8
FTO/ ZnO/$FAPbI_3$/CuSbS2	24.38	1.11	87.2	23.6

4.2.1. The nature of different HTMs band engineering

Figure 7 illustrates the band diagrams of the investigated solar cell with different HTM candidates.

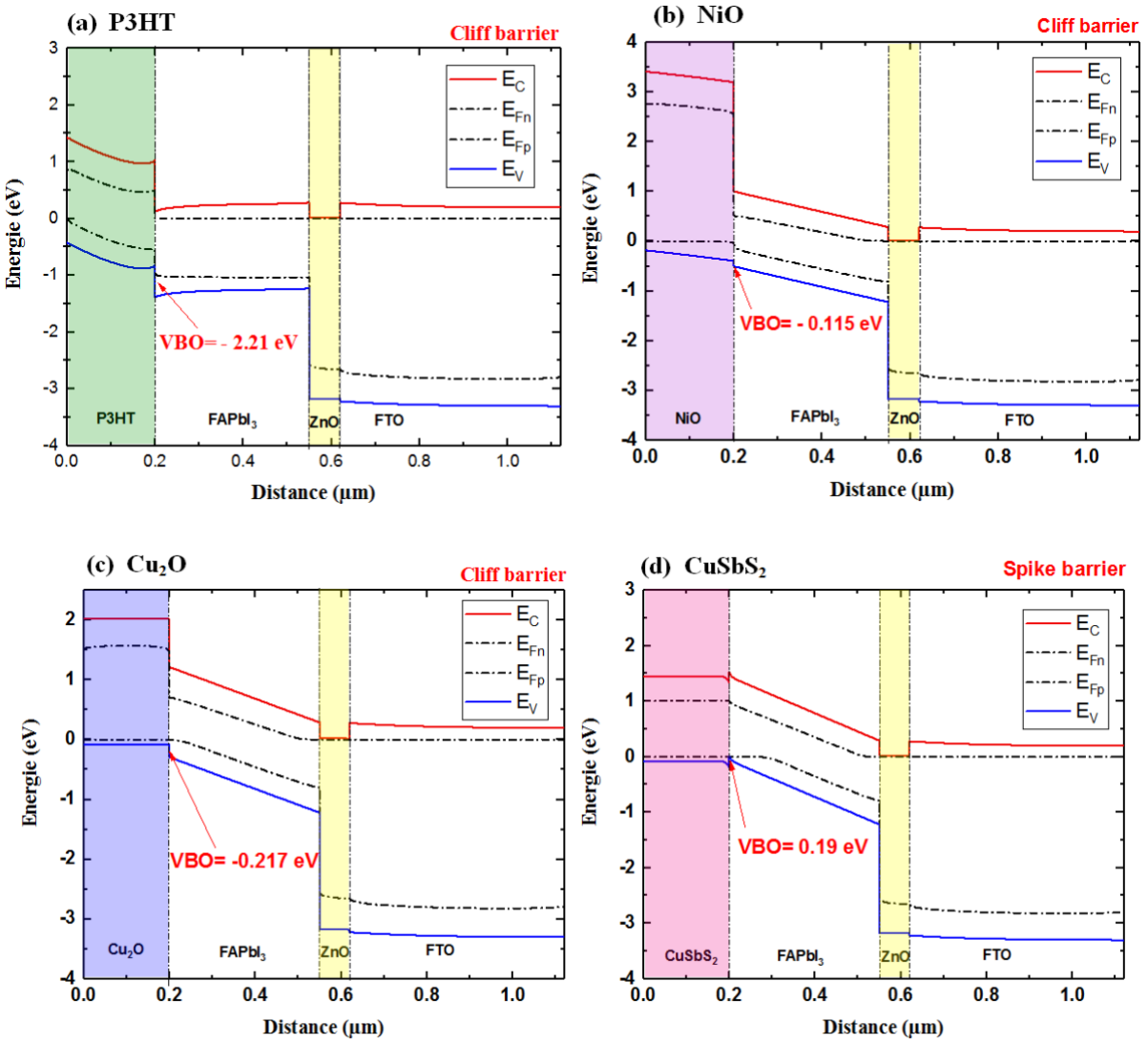

Figure 7 Band diagrams of different HTM candidates, (a) P3HT, (b) NiO, (c) Cu_2O, (d) $CuSbS_2$.

It can be seen from **figure 7** that a suitable valence band offset VBO^+ ($VB_{HTM}>VB_{PVK}$) is achieved when using $CuSbS_2$ as HTM however this material serves as a weak electron blocking layer when compared to NiO and Cu_2O. Organic P3HT and Spiro-OMeTAD exhibit a VBO^- which can hinder the conversion efficiency.

4.3. Optimized $(FAPbI_3)_{1-x}$ $(MAPbBr_3)_x$ perovskite solar cell

Notably, perovskite materials' compositional engineering has been widely used to modify their bandgap and structural characteristics for application in competitive PSCs. As an absorbent layer, $(FAPbI_3)_{1-x}$ $(MAPbBr_3)_x$ (x = 0.1–0.15) has been shown to boost the V_{OC} of solar cells and confirmed superior stability [33,34].

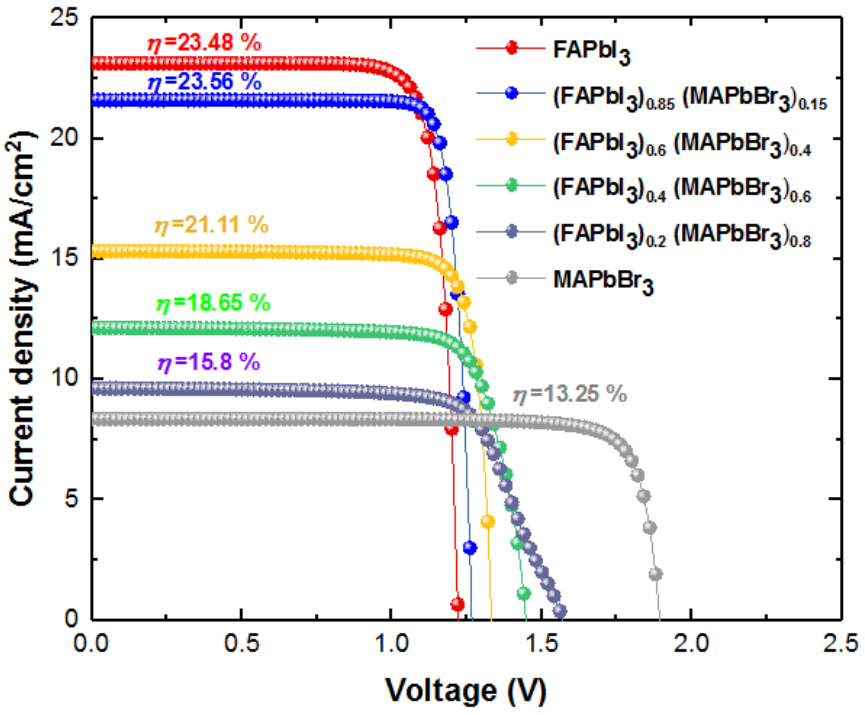

Figure 8. *I-V* characteristics of $(FAPbI_3)_{1-x}(MAPbBr_3)_x$ with different compositions.

Figure 8 depicts the *I-V* characteristics of $(FAPbI_3)_{1-x}(MAPbBr_3)_x$ with different compositions. It can be seen from this figure that as the fraction of $MAPbBr_3$ increases, J_{SC} is penalized. This fact is mainly due to the increased bandgap which hinders the absorption. On the contrary, the V_{OC} increases with increasing the $MAPbBr_3$ fraction, which make a tradeoff between both outputs. The best composition is $(FAPbI_3)_{0.85}(MAPbBr_3)_{0.15}$ for which an efficiency of 23.56 % is achieved.

Table 8 Electrical outputs of the investigated perovskite solar cell.

Structure	V_{OC} (V)	J_{SC} (mA/cm^{-2})	FF (%)	QE (%)
FTO/ZnO/$(FAPbI_3)_{0.85}(MAPbBr_3)_{0.15}$ /Cu_2O	1.267	23.56	86.08	23.56

Several theoretical and simulation investigations have shown that the optimal thickness of a perovskite layer for a single cation perovskite layer, like $FAPbI_3$, is 300-500 nm [35]. Determining the optimal thickness of the mixed cation-anion perovskite layer has a considerable influence on device performance. As a result, we examined the influence of perovskite thickness on PV performance employing ZnO and Cu_2O as CTL materials, respectively. When seen in **Figure 9**, as the thickness of the perovskite increases, the *FF* decreases monotonically in relation to the rising series resistance. At the same time, V_{OC} drops, which is attributed to the carriers' recombination rate increase in the presence of a larger absorber layer, resulting in a rise in saturation current greater than in photocurrent. A thick layer, otherwise, captures further light and therefore boosts charge carrier concentration, resulting in a high J_{SC} value. Following that, the *PCE* rises to a high of 25.74 percent at 800 nm thickness, after which it saturates and begins to fall. The transfer of charge carriers becomes longer as the absorber layer thickness rises, increasing the rate of recombination.

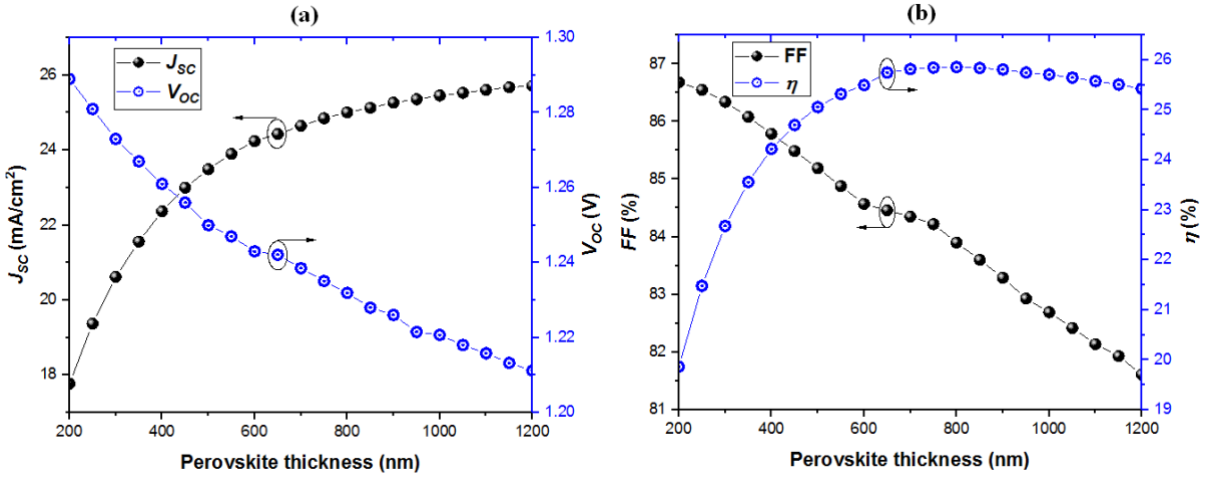

Figure. 9 Electrical outputs of the mixed cation perovskite $(FAPbI_3)_{0.85}(MAPbBr_3)_{0.15}$ solar cell versus the absorber layer thickness, (a) J_{SC}, V_{OC}, (b) *FF*, *PCE*.

It is worthy to note that adding $MAPbI_3$ improves the solar cell stability. However, the cliff-like conformation presented by the mixed perovskite/CTLs must be resolved by the band

offset engineering of both ETL and HTL materials, this fact will be investigated in the following section.

4.4. Mixed perovskite/CTLs band offset engineering

One of the PSCs community's concerns is band energy alignment between the absorbing material and CTLs. To overcome such difficulties, efforts should be made to establish a connection between theoretical and experimental research. Via the theoretical modeling detailed in section 2, we be able to see the creation of two structures linked to the CBO of ZnO/$(FAPbI_3)_{0.85}(MAPbBr_3)_{0.15}$ interface, which depend on the difference between electron affinities of ETL (EA_{ETL}) and absorber ($EA_{Absorber}$)), as depicted in **Figure 10**. The electron affinity of ZnO can be tuned via adding different Mg content. As showed in the figure, CBO(-) developed a cliff-like conformation, whereas CBO(+) created an energy spike-like conformation. i.e., if ETL's conduction band is lesser than the absorber's, the energy cliff CBO (-) is created, without any potential barrier for electrons. If ETL's conduction band is relatively high compared to that of perovskite, the spike-like conformation CBO (+) is established, operating as a electrons barrier, as depicted in Figure 14. The development of cliff-like conformation cause an accumulation close to ZnMgO/perovskite, which improves recombination in this location. The creation of spike-like conformation, on the other hand, decrease recombination at ZnMgO/$(FAPbI_3)_{0.85}(MAPbBr_3)_{0.15}$ by acting as band bending. Analogous phenomenon has been seen in PSCs as well as other thin-film solar cells [35-36]. Improved performance of PSCs requires also an appropriate energy band alignment at perovskite/ HTL interface. The difference between the absorber layer's valence band and that of HTM is considerable. As mentioned earlier, valence energy Ev ($EA_{Absorber}$-EA_{HTL})<0 is required to enhance the photovoltaic parameters [12]. We investigate the influence of VBO via adjusting the electron affinity (EA_{HTL}) of Cu2O to produce a deeper HTM level associated

with mixed perovskite material. Adjustment the electron affinity of Cu2O may improve the performance of the SC, as seen in **Figure 10.**

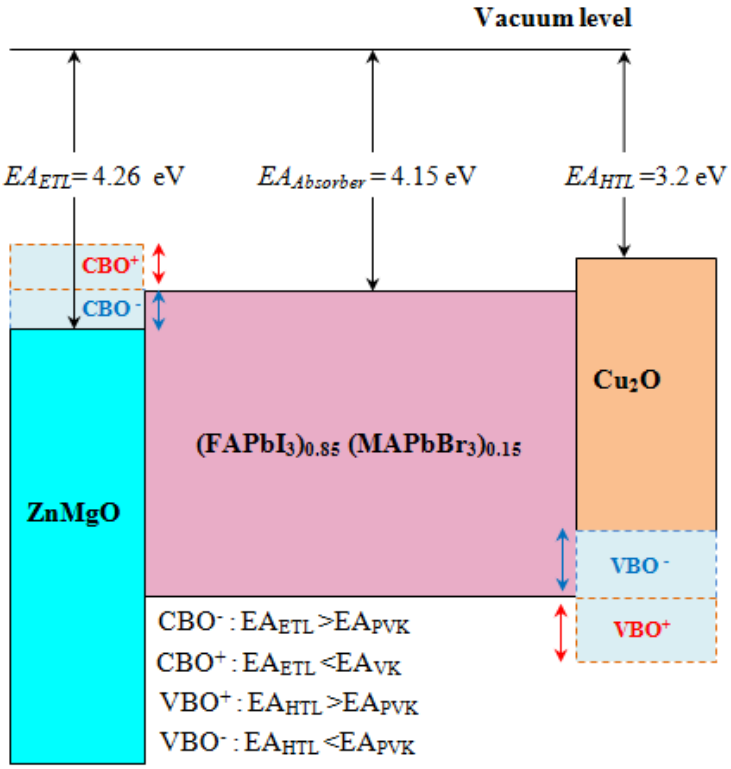

Figure 10 Band alignments of ZnMgO/Mixed perovskite with negative and positive CBOs and those of mixed perovskite /Cu_2O layers with negative and positive VBOs.

4.4.1 ETL/perovskite interface

Modified ZnO-doped with an optimum Mg concentration has a lot of promise for fabricating effective conduction bands and achieving the required spike structure. Mg treatment of ZnO has recently been demonstrated to improve electron extraction and minimize recombination in MAPbI3 [30]. An optimal conduction band (affinity) of ZnMgO (3.86 eV) may be achieved by adjusting the quantity of Mg doping. **Figure 11** depicts energy levels diagram (relative to the vacuum level) of ZnO films by varying the electron affinity of ZnO via adding different amounts of Mg (0.05-0.2) with respect to the absorber.

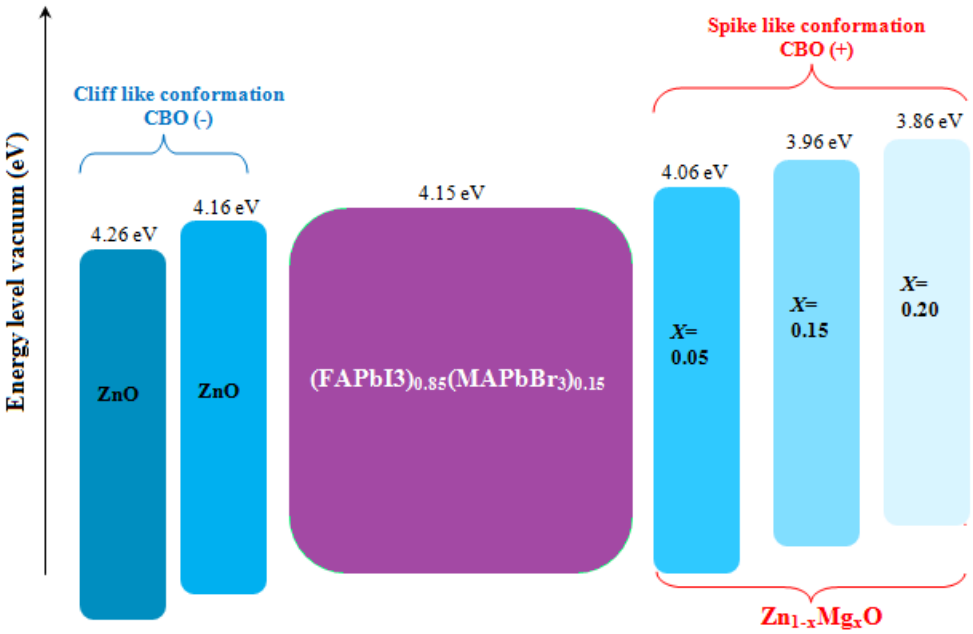

Figure 11 $Zn_{1-x}Mg_xO$ energy levels Diagram (relative to the vacuum level) (x=0-0.20).

Figure 12 depicts the impact of the *CBO* on the electrical outputs of the device. The cliff like conformation turns into a spike one when the *CBO* value increases (*CBO= EA*$_{PVK}$*-EA*$_{ETL}$).

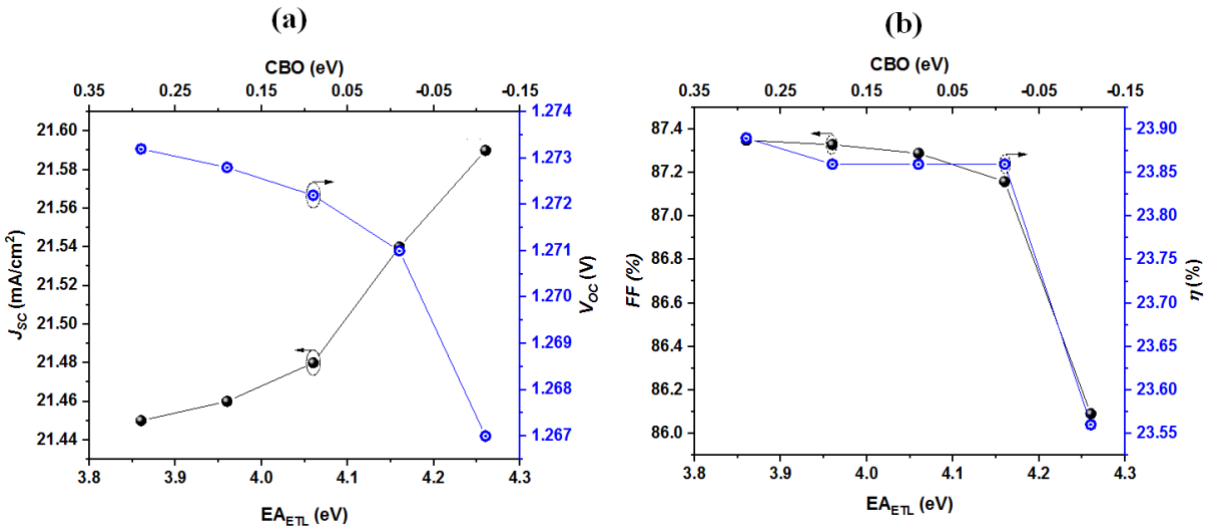

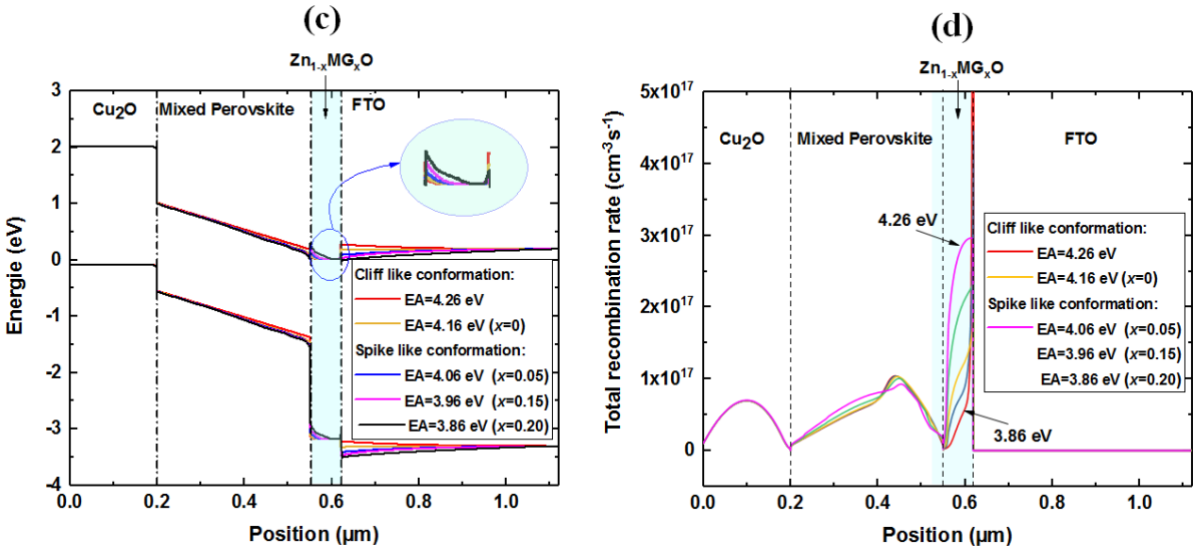

Figure 12 a) J_{SC} and V_{OC} as function of EA_{ETL} b) *FF* and *PCE* as function of EA_{ETL} c) Band diagram for different EA_{ETL} values d) Total recombination rate for different EA_{ETL} values.

It can be seen from **figure 12-a** that the J_{SC} raises slightly with increasing EA_{ETL}, in other hand, the more the EA_{ETL} increase the V_{OC} will be penalized, which is attributed to the transition of the band alignment structure from spike-like conformation (EA_{ETL} =3.86 eV, 3.96 eV, 4.06 eV) to cliff-like conformation (EA_{ETL}= 4.16 eV, 4.26 eV), this fact increases the electron-hole recombination effect due to the decreased potential difference, as it is illustrated in **figure 12-d**. In contrast, the creation of a spike structure causes the establishment of a barrier at ETL/mixed-perovskite that favors charge carrier separation. From figure **12-b** it can be seen that the EA_{ETL} have a slight effect on the *FF* and the efficiency till a value of ETL affinity equal 4.26 eV, which is attributed to the formation of cliff-type conformation, which in turn cause an increase recombination rate.

The solar cell with CBO^{+} = +0.29 eV (EA_{ETL}=3.86eV) and spike-like conformation performed the best, with a large *PCE* value of 23.86 percent, a V_{OC} of 1.274 V, a J_{SC} of 21.45 mA/cm^2, and a *FF* of 87.3 percent for a thickness of perovskite equal to 350 nm.

By studying the benefits of the spike-like structure generated at the ETL/absorber layer interface, it is clear that trying to avoid this structure will be ineffective since it works as a

barrier to block electrons to the back contact. Therefore, it increases the rate of recombination at the interface.

4.4.2. Perovskite/HTM interface

The impact of the VBO on photovoltaic characteristics of PSCs utilizing the optimal CBO (0.29 eV) for ZnMgO/mixed-perovskite as mentioned in the preceding section is shown in **Figures 13-a and 13-b**.

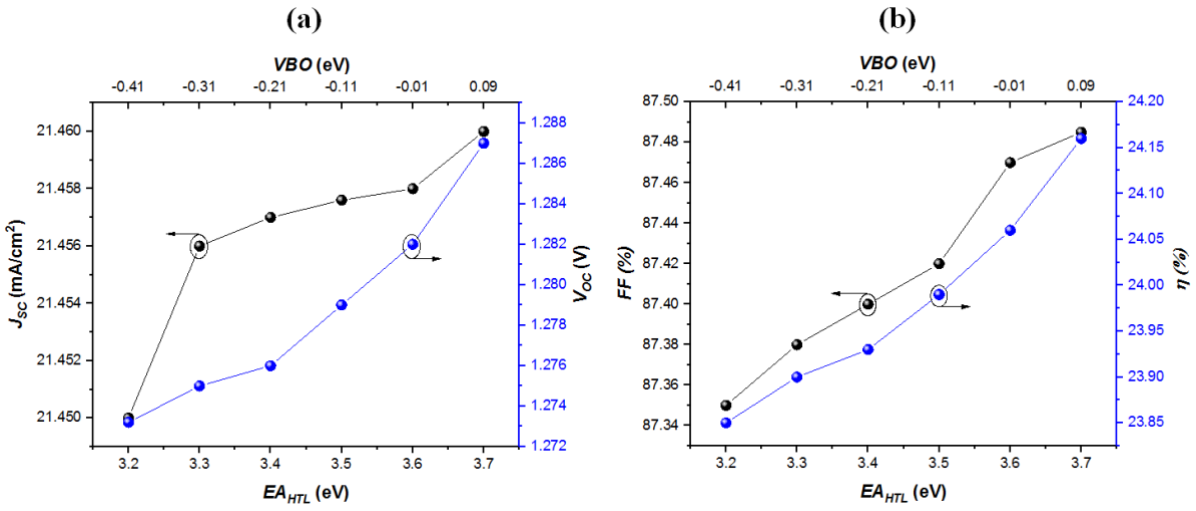

Figure 13 Electrical outputs of the investigated solar cell as function (CuO_2) affinity, (a) J_{SC}, V_{OC}, (b) *FF*, *PCE*.

When the HTL affinity EA_{HTL} increases more than 3.2 eV (V_{BO}^- = -0.41 eV), both *V*oc and *J*sc increase. In addition *FF* and *PCE* improved for increased EA_{HTL} values and reach the maximum for EA_{HTL} equal to 3.7 eV (VBO^+=0.09 eV) ($VBO = EA_{HTL}+Eg_{HTL}- (EA_{PVK} + Eg_{PVK}$). In our study, we determined the optimal value of EA_{HTL} to be 3.7 eV (VBO^+= 0.09 eV) while also determining the optimal value of EA_{HTL} to be 3.86 eV (CBO^+=0.29 eV). Based on these findings, we may improve the efficiency of PSCs by increasing the HTMs 'deep lower unoccupied molecule level (LUMO) in relation to the absorber layer. We attained this by utilizing Cu_2O as the HTM, but by optimizing its electron affinity (3.7 eV), which

theoretically can give a peak performance of 24.16 and 25. 86 percent for a thickness of perovskite equal to 350 nm and 800nm, respectively.

4.5. Optimized back contact work function

Because of its high efficiency and cheap manufacturing cost, organic–inorganic halide PSCs have deserved the attention of many researchers. Back contact metals such as Au and Ag are commonly utilized. However, they show limitations such as Au being expensive and Ag being unstable when exposed to the environment. In this study, Au, Ni, Cu, Mo, W, Al and Ag illustrated in **figure 14** were considered as back contact electrodes for PSCs. We investigated how metals' work functions impact their photovoltaic properties.

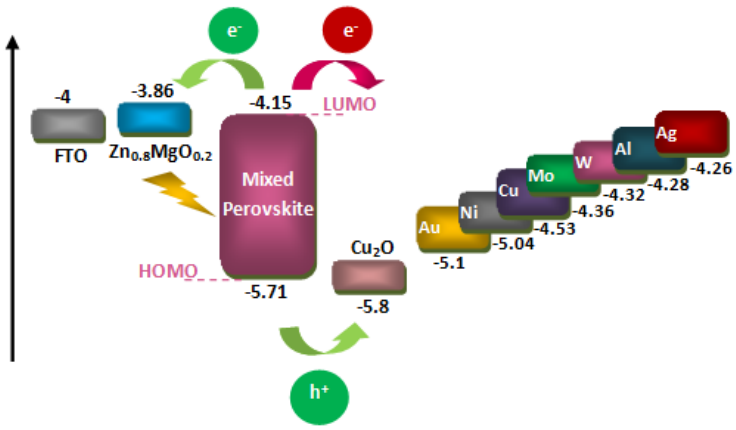

Figure 14. Optimized alignment of the energy band diagrams for perovskite with different metal contact candidates.

Figures 15-a and **15-b** showed the electrical outputs of our simulated solar cell (extracted from **Figures 15-c**) terminated with different back contact. The performance of PSCs initially improves with raising metals work function till a specific value of 5.04 eV, beyond which it saturates.

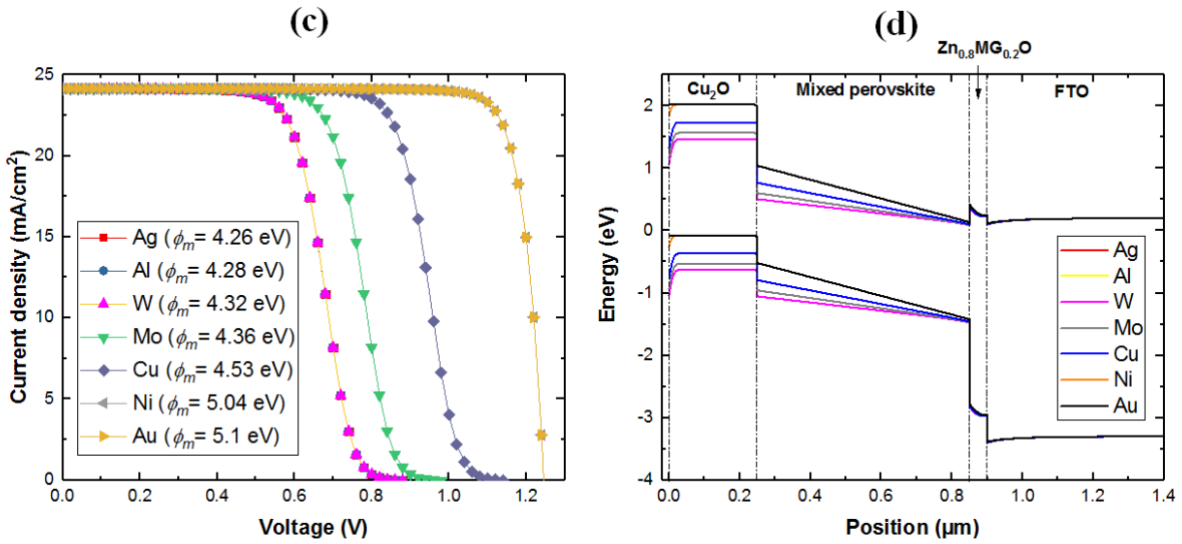

Figure 15 Electrical outputs for different metal work function values a) J_{SC} and V_{OC} b) *FF* and *PCE* c) *J-V* characteristics d) Band diagrams.

Because of band bending at the metal-semiconductor interface, the Fermi level energy drops when utilizing a metal with a higher work function value, rendering the contact more ohmic [38]. Based on the metal work function values shown in **Figure 14** for various back contacts, we suggest that Ni, with a work function of 5.04 eV, should be an efficient option to substitute the expensive Au electrode. An efficiency of 25.86%, for perovskite thickness of 350 nm, can be reached by using structure FTO/ZnMgO/$(FAPbI_3)_{0.85}$ $(MAPbBr_3)_{0.15}$/Cu_2O/Ni for low cost PSCs.

4.6. Optimized FTO/$Zn_{0.8}Mg_{0.2}O$/$(FAPbI_3)_{0.85}$ $(MAPbBr_3)_{0.15}$/Cu_2O/Ni structure

Table 7 presents a comparison of the optimized and conventional PSCs. It illustrates the design structure's capability in improving the PSC without compromising the conversion efficiency. This is possible by employing efficient CTLs materials and an appropriate band engineering offset. The comparison clearly shows that the suggested solar cell (see last column in Table 9) is capable of producing superior outcomes, making it an appealing alternative.

Table 9 Comparison between optimized perovskite solar cell and conventional structures.

Design parameters	Experiment al work [13]	Conventional solar cell (simulated)	Optimized perovskite solar cell
ETL material	SnO_2	SnO_2	$Zn_{0.8}Mg_{0.2}O$
Dopping concentration (cm^{-2})	10^{15}	10^{15}	10^{17}
Thickness	70	70	50
Affinity (eV)	4	4	3.86
CBO (eV)	0	0	0.29
HTL material	Spiro-OMeTAD	Spiro-OMeTAD	Cu_2O
Doping concentration (cm^{-2})	10^{18}	10^{18}	10^{18}
Thickness	200	200	250
Affinity (eV)	2.2	2.2	3.7
VBO (eV)	-0.38	-0.38	0.09
Perovskite material	$FAPbI_3$	$FAPbI_3$	$(FAPbI_3)/(MAPbBr_3)$
$MAPBrI_3$ ratio (%)	0	0	15
Band gap	1.51	1.51	1.56
Affinity (eV)	4	4	4.15
Thickness	350	350	350
Electrode	Au	Au	Ni
work function (eV)	5.1	5.1	5.04
Output parameters			
J_{SC} (mA/cm^2)	22.6	22.96	25.01
V_{OC} (V)	1.2	1.21	1.23
FF	77	79.17	83.9
Efficiency (%)	21.4	22.17	25.86

Conclusion

The $FAPbI_3$ absorber-based PSC is numerically investigated and optimized using SCAPS-1D software package. Initially, a variety of potential inorganic materials for CTL are investigated. Cu_2O HTL outperforms other choices; hence it is regarded as the best candidate for HTL in $FAPbI_3$ i-PSCs. For ETLs, SnO_2, TiO_2 and ZnO provides similar conversion efficiency when implemented as ETLs, owing to its elevated transparence and high conductivity. In order to boost the performance of the investigated solar cell, FAPbI3 solar cell with different $MAPbBr_3$ amounts is examined. Hybrid $(FAPbI3)_{0.85}(MAPbBr3)_{0.15}$ presents the optimal performance where an efficiency of 23.56 % is reached. Besides, we analyze the absorber thickness influence on the performance of the solar cell. To decrease interfacial recombination in PSCs, energy level engineering is critical. Accordingly, we study the impact of the conduction band offset (CBO) in PSC by varying the Mg content to locate the appropriate electronic properties of ZnO (conductivity and electron affinity). We discovered that an appropriate value of the conduction band offset (CBO^+ =0.29) assures a “spike-type" band alignment. This choice lowers the unwanted recombination mechanism at the $Zn_{0.8}Mg_{0.2}O$ /$(FAPbI_3)_{0.85}(MAPbB_3)_{0.15}$ interface, resulting in a challenging PCE with an optimized C_{BO} of 0.29 eV. Cu_2O's adjusted V_{BO}^+ was determined to be 0.09 eV. In addition, the impact of the back contact work function is investigated. According to simulation findings, Ni back electrodes with a work function of 5.04 eV is appropriate for $Zn_{0.8}Mg_{0.2}O$ /$(FAPbI3)_{0.85}(MAPbB3)_{0.15}/Cu_2O$ i-PSCs. For mixed perovskite based i-PSCs, an optimal efficiency of 25.86 percent may be attained after extensive optimization. The simulation results are useful in better clarifying and enhancing the performance of perovskite solar cells based on $FAPbI_3$.

References

[1] H. Min, D. Y. Lee, J. Kim, G. Kim, K. S. Lee, J. Kim, S. Il Seok, "Perovskite solar cells with atomically coherent interlayers on SnO2 electrodes". Nature, vol. 598(7881), pp. 444-450, 2021.

[2] P. Roy, N. K. Sinha, S. Tiwari, A. Khare, "A review on perovskite solar cells: Evolution of architecture, fabrication techniques, commercialization issues and status". Solar Energy, vol. 198, pp. 665-688, (2020).

[3] C. H. Ng, H. N. Lim, S. Hayase, Z. Zainal, N. M. Huang, "Photovoltaic performances of mono-and mixed-halide structures for perovskite solar cell: A review". Renewable and Sustainable Energy Reviews, vol. 90, pp. 248-274, 2018.

[4] J. Wang, J. Zhang, Y. Zhou, H. Liu, Q. Xue, , X. Li, A. K. Jen, « Highly efficient all-inorganic perovskite solar cells with suppressed non-radiative recombination by a Lewis base". Nature communications, vol. 11(1), pp. 1-9, 2020.

[5] M. Stolterfoht, C. M. Wolff, J. A. Márquez, S. Zhang, C. J. Hages, D. Rothhardt, D. Neher, "Visualization and suppression of interfacial recombination for high-efficiency large-area pin perovskite solar cells". Nature Energy, vol. 3(10), pp. 847-854, 2018.

[6] F. Giordano, A. Abate, J. P. C. Baena, M. Saliba, T. Matsui, S. H. Im, M. Graetzel, "Enhanced electronic properties in mesoporous TiO 2 via lithium doping for high-efficiency perovskite solar c ells". Nature communications, vol. 7(1), pp. 1-6, 2016.

[7] Y. Shao, Z. Xiao, C. Bi, Y. Yuan, J. Huang, "Origin and elimination of photocurrent hysteresis by fullerene passivation in CH 3 NH 3 PbI 3 planar heterojunction solar cells". Nature communications, vol. 5(1), pp. 1-7, 2014.

[8] X. Ren, D. Yang, Z. Yang, J. Feng, X. Zhu, J. Niu, S. F. Liu, "Solution-processed Nb: SnO2 electron transport layer for efficient planar perovskite solar cells . ACS applied materials & interfaces, vol. 9(3), pp. 2421-2429, 2017.

[9] K. T. Cho, S. Paek, , G. Grancini, C. Roldán-Carmona, P. Gao, Y. Lee, M. K. Nazeeruddin, "Highly efficient perovskite solar cells with a compositionally engineered perovskite/hole transporting material interface". Energy & Environmental Science, vol. 10(2), pp. 621-627, 2017.

[10] D. B. Khadka, Y. Shirai, M. Yanagida,J. W. Ryan, K. Miyano, "Exploring the effects of interfacial carrier transport layers on device performance and optoelectronic properties of planar perovskite solar cells". Journal of Materials Chemistry C, vol. 5(34), pp. 8819-8827, 2017.

[11] T. Minemoto, M. Murata, "Theoretical analysis on effect of band offsets in perovskite solar cells", Solar Energy Materials Solar Cells, vol.133, pp. 8, 2015.

[12] L. Lin, L. Jiang, P. Li, B. Fan, Y. Qiu, "A modeled perovskite solar cell structure with a Cu2O hole-transporting layer enabling over 20% efficiency by low-cost low-temperature processing." Journal of Physics and Chemistry of Solids, vol. 124, pp. 205-211, 2019.

[13] S. Karthick, S. Velumani, J. Bouclé, "Experimental and SCAPS simulated formamidinium perovskite solar cells: a comparison of device performance". Solar Energy, vol. 205, pp. 349-357, 2020.

[14] M. Burgelman, K. Decock, A. Niemegeers, J. Verschraegen, S. Degrave, SCAPS Manual, 2018. Version.

[15] Y. Raoui, H. Ez-Zahraouy, S. Kazim, S. Ahmad, "Energy level engineering of charge selective contact and halide perovskite by modulating band offset: Mechanistic insights". Journal of Energy Chemistry, vol. 54, pp. 822-829, 2021.

[16] N. J. Jeon, J. H. Noh, W. S. Yang, Y. C. Kim, S. Ryu, J. Seo, S. I. Seok, "Compositional engineering of perovskite materials for high-performance solar cells". Nature, vol .517(7535), pp. 476-480, 2015.

[17] L.C. Chen, Z.L. Tseng, J.K. Huang, "A study of inverted-type perovskite solar cells with various composition ratios of (FAPBI3)1–x(MAPbBr 3)x". Nanomaterials, , 2016. https:// doi.org/10.3390/nano6100183.

[18] F. Ma, J. Li, W. Li, N. Lin, L. Wang, J. Qiao, "Stable α/δ phase junction of formamidinium lead iodide perovskites for enhanced near-infrared emission". Chem, 2016. Sci. https://doi.org/10.1039/c6sc03542f.

[19] M.C. Gélvez-Rueda, N. Renaud, F.C. Grozema, "Temperature dependent charge carrier dynamics in formamidinium lead iodide perovskite". J. Phys. Chem. C. 2017. .https:// doi.org/10.1021/acs.jpcc.7b09303.

[20] N. Onoda-Yamamuro, T. Matsuo, H. Suga, "Dielectric study of CH3NH3PbX3 (X = Cl, Br, I)". J. Phys. Chem. Solids, vol. 53, pp. 935–939, 1992.

[21] F. Zu, P. Amsalem, D. A. Egger, R. Wang, C. M. Wolff, H. Fang, N. Koch, "Constructing the electronic structure of CH3NH3PbI3 and CH3NH3PbBr3 perovskite thin films from single-crystal band structure measurements". The journal of physical chemistry letters, vol. 10(3), pp. 601-609, 2019.

[22] M. Born, E. Wolf, "Principles of optics: electromagnetic theory of propagation, interference and diffraction of light", Elsevier, 2013.

[23] M. Kato, T. Fujiseki, T. Miyadera, T. Sugita, S. Fujimoto, M. Tamakoshi, H. Fujiwara, "Universal rules for visible-light absorption in hybrid perovskite materials". Journal of Applied Physics, vol. 121(11), pp. 115501, 2017.

[24] T. Bendib, H. Bencherif, M. A. Abdi, F. Meddour, L. Dehimi, M. Chahdi, "Combined optical-electrical modeling of perovskite solar cell with an optimized design". Optical Materials, vol. 109, pp. 110259, 2020.

[25] H. Bencherif, "Towards a high efficient Cd-free double CZTS layers kesterite solar cell using an optimized interface band alignment". Solar Energy, vol. 238, pp. 114-125, 2022.

[26] N. F. Ramli, P. N. A. Fahsyar, N. A. Ludin, M. A. M. Teridi, M. A. Ibrahim, S. H. Zaidi, S. Sepeai, "Compatibility between compact and mesoporous TiO2 layers on the optimization of photocurrent density in photoelectrochemical cells". Surfaces and Interfaces, vol. 17, pp. 100341, 2019.

[27] N. Rai, S. Rai, P. K. Singh, P. Lohia, D. K. Dwivedi, "Analysis of various ETL materials for an efficient perovskite solar cell by numerical simulation". Journal of Materials Science: Materials in Electronics, vol. 31(19), pp. 16269-16280, 2020.

[28] M. H. Elshorbagy, A. Cuadrado, B. Romero, J. Alda, "Enabling selective absorption in perovskite solar cells for refractometric sensing of gases". Scientific reports, vol. 10(1), pp. 1-11, 2020.

[29] Y. Raoui, H. Ez-Zahraouy, N. Tahiri, O. El Bounagui, S. Ahmad, S. Kazim, "Performance analysis of MAPbI3 based perovskite solar cells employing diverse charge selective contacts: Simulation study". Solar Energy, vol. 193, pp. 948-955, 2019.

[30] C. Ding, Y. Zhang, F. Liu, Y. Kitabatake, S. Hayase, T. Toyoda, Q. Shen, "Effect of the conduction band offset on interfacial recombination behavior of the planar perovskite solar cells". Nano Energy, vol. 53, pp. 17-26, 2018.

[31] L. Meng, J. You, Y. Yang, "Addressing the stability issue of perovskite solar cells for commercial applications". Nature communications, vol. 9(1), pp. 1-4, 2018.

[32] L. Xu, R.M. Imenabadi, W. G. Vandenberghe, J. W. Hsu, « Minimizing performance degradation induced by interfacial recombination in perovskite solar cells through

tailoring of the transport layer electronic properties". APL Materials, vol. 6(3), pp. 036104, 2018.

[33] J. Wang, F.Meng, R. Li, S. Chen, X. Huang, J. Xu, H. L. Wang, "Boosting Efficiency and Stability of Planar Inverted (FAPbI3) x (MAPbBr3) 1− x Solar Cells via FAPbI3 and MAPbBr3 Crystal Powders". Solar RRL, vol. 4(5), pp. 2000091, 2020.

[34] Y. Reyna, M. Salado, S. Kazim, A. Perez-Tomas, S. Ahmad, M. Lira-Cantu, "Performance and stability of mixed FAPbI3 (0.85) MAPbBr3 (0.15) halide perovskite solar cells under outdoor conditions and the effect of low light irradiation". Nano Energy, vol. 30, pp. 570-579, 2016.

[35] M. B. Kanoun, A. A. Kanoun, A. E. Merad, S. Goumri-Said, "Device design optimization with interface engineering for highly efficient mixed cations and halides perovskite solar cells". Results in Physics, vol. 20, pp. 103707, 2021.

[36] H. Zhou, Q. Chen, G. Li, S. Luo, T. B. Song, H. S. Duan, Y. Yang, "Interface engineering of highly efficient perovskite solar cells". Science, vol. 345(6196), pp. 542-546, 2014.

[37] H. Bencherif, L. Dehimi, N. Mahsar, E. Kouriche, F. Pezzimenti, "Modeling and optimization of CZTS kesterite solar cells using TiO2 as efficient electron transport layer". Materials Science and Engineering: B, vol. 276, pp. 115574, 2022.

[38] F. Behrouznejad, S. Shahbazi, N. Taghavinia, H.P. Wu, E.W.G. Diau, "A study on utilizing different metals as the back contact of CH 3 NH 3 PbI 3 perovskite solar cells". J. Mater. Chem. A , vol. 4 (35), pp. 13488–13498, 2016.